Eur. Phys. J. A (2023) 59:144
https://doi.org/10.1140/epja/s10050-023-01032-5

THE EUROPEAN PHYSICAL JOURNAL A

Regular Article - Experimental Physics

AGATA: nuclear structure advancements with fusion-evaporation reactions

G. de Angelis[1], G. Benzoni[2], B. Cederwall[3], A. Korichi[4], S. Leoni[2,5,a], A. López-Martens[4], J. Nyberg[6], E. S. Paul[7], J. J. Valiente-Dobòn[1,b]

[1] Laboratori Nazionali di Legnaro, Istituto Nazionale di Fisica Nucleare (INFN), Legnaro, Italy
[2] Istituto Nazionale di Fisica Nucleare (INFN), Sezione di Milano, Milano, Italy
[3] Department of Physics, KTH Royal Institute of Technology, Stockholm, Sweden
[4] Université Paris-Saclay, CNRS/IN2P3, IJCLab, Orsay, France
[5] Dipartimento di Fisica, Università degli Studi di Milano, Milano, Italy
[6] Department of Physics and Astronomy, Uppsala University, Uppsala, Sweden
[7] Department of Physics, University of Liverpool, Liverpool L69 7ZE, UK

Received: 14 March 2023 / Accepted: 13 May 2023 / Published online: 3 July 2023

Communicated by Nicolas Alamanos

Abstract Nuclear-structure studies using fusion reactions are reviewed in terms of prospects for advancement using the next generation of γ-ray tracking arrays such as AGATA. Properties discussed include those of light $N = Z$ nuclei and rotational behaviour in heavy nuclei at high values of angular momentum and internal excitation energy.

1 Introduction

The fusion-evaporation reaction has long been a mainstay of nuclear-structure physics. This reaction mechanism brings in large amounts of excitation energy and angular momentum to the nucleus. Low-energy nuclear accelerator facilities provide heavy-ion beams with energies from about 3 to 5 MeV per nucleon to initiate the fusion process and the primary detection is of the decay γ rays of the excited nuclei. In addition to stable beam species, new ISOL as well as fragmentation facilities can now also provide radioactive ion beams to help in the study of exotic nuclei far away from the valley of stability.

The physics results discussed in this paper are given in the context of the evolution of multi-detector γ-ray spectrometers, culminating in the future highly efficient AGATA [1–5] and GRETA [6] 4π shells of hyperpure, electrically segmented, germanium (Ge) semiconductor detectors.

2 Structure of $N = Z$ nuclei

Beyond the heaviest stable, self-conjugate ($N = Z$) nucleus, $^{40}_{20}Ca_{20}$, which is also a doubly magic system, the valley of beta stability starts to depart more and more rapidly away from the $N = Z$ line. Consequently, the heavier $N \approx Z$ nuclei become successively more and more unstable, up to the doubly-magic nucleus $^{100}_{50}Sn_{50}$, the most massive self-conjugate nucleus predicted to be bound. Near-self-conjugate nuclei possess special properties since neutrons and protons move in identical orbits. They are important for studying isospin symmetry breaking effects in the nuclear Hamiltonian and the competion between different isospin components of nucleon-nucleon pairing forces. These effects are expected to become more pronounced along the $N = Z$ line with increasing mass while, at the same time, nuclei become less bound and therefore also more difficult to reach experimentally. For the most exotic nuclei, pairing correlations can no longer be treated as a small residual interaction as they approach the same order of magnitude as the binding energy of valence nucleons generated from the remaining part of the nuclear potential.

2.1 Isospin symmetry tests

Symmetries in physical laws are particularly important for our understanding of their nature and consequences. They, either exact or only approximate, play an essential role in the fields of elementary particle and nuclear physics. The fact that nuclear forces are about the same exchanging protons with neutrons (charge symmetry) and that they are almost

[a] e-mail: silvia.leoni@mi.infn.it (corresponding author)
[b] e-mail: javier.valiente@lnl.infn.it

the same with sequential exchange of a neutron for a proton (charge independence) allows us to treat protons and neutrons as different states of the same particle (the nucleon) and to classify nuclear states according to the different representation of a symmetry group, the isospin SU(2). This may be stated as hadronic forces are invariant under rotation in isospin space and is ultimately related to the near degeneracy of up and down quarks [7]. Charge independence is roughly true if we consider that the nuclear force, at least when measured in free space, is not quite charge symmetric—that is, the neutron-neutron interaction is just a bit stronger than the proton-proton interaction (the nucleon-nucleon scattering lengths are $a_{pp} = -17.7(0.4)$ fm, $a_{nn} = -18.8(0.3)$ fm and $a_{np} = -23.75 \pm 0.09$ fm). It is also of interest how this "charge-asymmetry", and any other "isospin-violating" forces, manifest in the nuclear medium.

Isospin symmetry was the first internal symmetry (as distinguished from space-time symmetries) to be postulated, initially for neutrons and protons and soon after for mesons as well. Under isospin symmetry, the proton and the neutron can be considered as two states of the same particle, referred to as the nucleon. They are characterised by the isospin quantum number $T = 1/2$, with a third component $T_3 = +1/2$ and $-1/2$, respectively. States of nuclei with the same mass number A can be grouped, according to the value of the isospin T, in isospin multiplets of $2T + 1$ states belonging to the different nuclei, distinguished by the value of $T_3 = (N - Z)/2$. For a pair of mirror nuclei, where the number of neutrons in one matches the number of protons in the other, one therefore may expect their properties to be essentially the same. Isospin symmetry is manifestly violated by electromagnetic force as the proton has a positive charge and the neutron is neutral. However, the most important part of the Coulomb interactions are diagonal with respect to T_3 and mainly contributes to the mass difference among various members of the isospin multiplet.

Since the electrostatic repulsion between protons is well understood, its effects on the nucleons can be calculated precisely and so any other significant differences observed for mirror nuclei may be attributed to other elusive forces that violate isospin symmetry. Isospin symmetry is also violated, to a lesser extent, by nuclear forces. Finer effects of the symmetry-breaking forces can be investigated by measuring the so-called mirror energy differences [8] or, more generally, differences in excitation energies among members of a multiplet. In recent years, a considerable number of experimental and theoretical studies have been dedicated to this subject, as excited states of nuclei with $T_3 = +1/2$, +3/2 could be measured for increasingly larger values of A. Furthermore, when transition probabilities are accessible, their comparison between mirror nuclei offers the possibility to investigate the amount and the origin of isospin violation. Here, we focus to the relatively simple case of $E1$ transitions [9].

The $E1$ transition operator is expected to be pure isovector, at least in the limit of long wavelengths, where Siegert's theorem [10] holds. This fact implies that (1) $E1$ transitions with $\Delta T = 0$ in nuclei with $N = Z$ are forbidden and that (2) corresponding $E1$ transitions in mirror nuclei have equal reduced strength. Both rules are to some extent violated by isospin-non conserving (mainly, Coulomb) interactions. In the $N = Z$ case, these violations appear as second-order effects, while in mirror nuclei the effect is of first order. The difference is due to the interference between the irregular amplitude (symmetric with respect to the exchange of the two nuclei in the doublet) with the regular amplitude (which is isovector antisymmetric with respect to the exchange). Violation of such selection rules can be used to test quantitatively the validity of isospin conservation. The breaking of isospin symmetry induces a mixing between states with different isospin values.

Testing the amount of isospin mixing is also important for a precise information on the weak interaction in β-decay which involves the up and down quarks. The study of $0^+ \rightarrow 0^+$ nuclear β decays plays an important role in our current understanding of the electroweak interaction. These transitions are now well known in the decays of a wide range of nuclei from ^{10}C to ^{74}Rb. Considered together, they probe the conservation of the vector current, set tight limits on the possible presence of scalar currents, and provide the most precise value for $|V_{ud}|$, the up-down quark-mixing element of the Cabibbo-Kobayashi-Maskawa (CKM) matrix. The value of such mixing element is an essential aspect in the most demanding available test of the unitarity of the CKM matrix: that the sum of squares of the top-row elements should equal unity. Since the axial current cannot contribute in first order to transitions between spin-0 states, superallowed $0^+ \rightarrow 0^+$ β-decay between $T = 1$ analog states depends uniquely on the vector part of the weak interaction. Thus, according to the conserved vector current (CVC) hypothesis, the experimental ft value for such a transition should be directly related to the vector coupling constant, GV, a fundamental constant, which must be the same for all such transitions. In practice, the ft values are subject to several small ($\approx 1\%$) correction terms, provided by theory, and one of them is the isospin-symmetry-breaking correction δc, depending on the details of nuclear structure.

Figure 1, taken from Ref. [11], shows the amount of isospin mixing α^2 as a function of the mass number calculated in the context of different theories (Density Functional theories) and of the isospin mixing correction δc as a function of the mass number calculated in the context of different theories. Figure 2 from Ref. [12] shows the matrix elements $|V_{ud}|$ (left panel) deduced from the superallowed $0^+ \rightarrow 0^+$ β-decay (dots) by using values of δc from different calculations. Triangles mark values obtained from the pion-decay and neutron-decay studies. The open circle shows the value

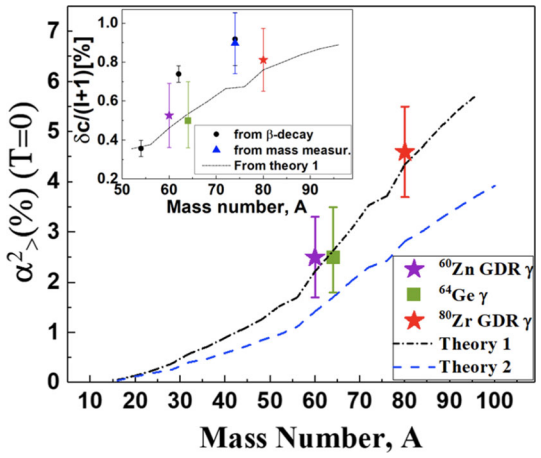

Fig. 1 Isospin mixing α^2 and isospin mixing correction δc as a function of the mass number calculated in the context of different density functional theories (DFT). Stars and squares are experimental values obtained using forbidden $E1$ transitions. Taken from Ref. [11]

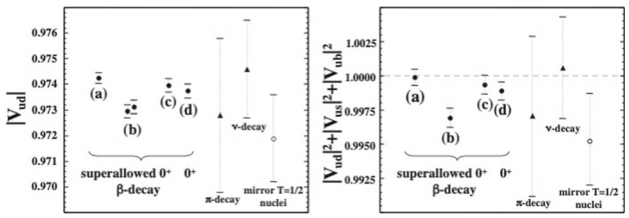

Fig. 2 Matrix elements $|V_{ud}|$ (left panel) deduced from the superallowed $0^+ \rightarrow 0^+$ β-decays (dots) by using values of δc from different calculations [12,13]. Triangles mark values obtained from the pion-decay and neutron-decay studies. The open circle shows the value of $|V_{ud}|$ deduced from the β-decays in the $T = 1/2$ mirror nuclei. The right panel shows the unitarity condition for different values of $|V_{ud}|$. Taken from Ref. [12]

of $|V_{ud}|$ deduced from the β-decays in the $T = 1/2$ mirror nuclei. The right panel shows the unitarity condition for different values of $|V_{ud}|$.

As already reported, one of the most direct ways of studying the violation of isospin symmetry induced by the Coulomb interaction (and other isospin breaking terms of the nuclear interaction) is the observation of $E1$ transitions in even–even $N = Z$ nuclei. In the long-wavelength limit, the matrix elements of the nuclear $E1$ operator vanish when both the initial and final states have equal isospin T and $T_3 = 0$ [9]. This is typically the case for the low-lying levels in even–even $N = Z$ nuclei, where electric dipole transitions should therefore be forbidden. However, the Coulomb interaction induces an admixture between these low-lying $T = 0$ states and the higher-lying $T = 1$ states of the same configuration having the same spin and parity. Electric dipole transitions are thus allowed between the $T = 0$ ($T = 1$) component of the initial state and the $T = 1$ ($T = 0$) component of the final one. The observed $E1$ strength is, therefore, a signature of the isospin mixing.

(a) Experimentally, isospin mixing can be tested by studies of low-lying $E1$ forbidden decays in $N = Z$ nuclei. Here the Coulomb interaction (and other isospin breaking terms of the nuclear interaction) induces an admixture between these low-lying $T = 0$ states and the higher-lying $T = 1$ states of the same configuration having the same spin and parity. Electric dipole transitions are thus allowed between the $T = 0$ ($T = 1$) component of the initial state and the $T = 1$ ($T = 0$) component of the final one. The observed $E1$ strength is, therefore, a signature of the isospin mixing. One notable example is the $N = Z$ nucleus ^{64}Ge which has been investigated in two experiments using the Euroball III and Euroball IV spectrometers coupled to ancillary devices.
As reported in Ref. [14], the precise determination of the angular distribution, linear polarisation and lifetime measurements are required for the precise determination of the $B(E1)$ strength. The results obtained for ^{64}Ge have determined unambiguously the multipole character of the $5^- \rightarrow 4^+$ 1665 keV transition, allowing the extraction of the electric dipole strength and the amount of isospin mixing of $\alpha^2 = 2.50\%$ $(+1.0\%, -0.7\%)$ [14]. This value is reported in Fig. 1 and is consistent with recent DFT theoretical calculations allowing one to probe the validity of this model for $A = 64$. Another interesting case is for $A = 72$. Two "forbidden" $E1$ transitions have been identified in the $N = Z = 36$ ^{72}Kr nucleus, a $(5^-) \rightarrow 4^+$ transition of 1134 keV and a $(3^-) \rightarrow 2^+$ of 1139 keV [15]. They both have a measured intensity of 5% relative to the $2^+ \rightarrow 0^+$ g.s. transition and for both an $(E1)$ character has been suggested [15,16]. The measurement of such $E1$ strengths in one of the heaviest $N = Z$ system presently achievable with sufficient statistics represents an interesting perspective using a position-sensitive gamma-ray detector array like AGATA, particularly suited for precise linear polarisation and lifetime measurements.

(b) The γ decay of the Giant Dipole Resonance (GDR) in $N = Z$ nuclei: The technique consists of detecting the $E1$ decay in nuclei with $N = Z$, forbidden unless there is a mixing of states with different isospin values. Since these mixings are rather small, the GDR, comprising almost 100% of the $E1$ strength, represents a good probe to search for forbidden decays and to find a signature of the isospin mixing in nuclear states.
The approach is to form, via fusion reactions, compound nuclei at finite temperature and then deduce isospin mixing at zero temperature by using the model reported in Ref. [17]. In heavy-ion reactions around the Coulomb barrier using self-conjugate projectiles and target nuclei, both with an equal number of protons and neutrons, the compound nucleus has $N = Z$ and thus is populated with isospin $T = 0$ and can decay by $E1$ transitions only

to states with isospin $T = 1$, characterised by a level density lower than that of $T = 0$ states. However, if the initial state has some degree of isospin mixing (and thus a small $T = 1$ component), its $E1$ decay to the more numerous $T = 0$ states can occur. Results on ^{80}Zr and ^{60}Zn have been recently published [11,17] and are shown in Fig. 3. For ^{80}Zr, presently the heaviest system where isospin mixing has been determined, the AGATA mutidetector array coupled to the LaBr2 scintillators of the HECTOR+ detector was used. A value of $\alpha^2 = 4.6 \pm 0.9\%$ was determined, see Fig. 4. For the nucleus ^{60}Zn, the isospin mixing probability at zero temperature was found to be $\alpha^2 = 2.5 \pm 0.8\%$, in very good agreement with the ^{64}Ge result [17].

(c) $E1$ strengths in mirror ($T_3 = 1/2, -1/2$) nuclei have to be identical under isospin conservation. Deviations from this rule appear through the presence of an induced isoscalar component (which is forbidden for $E1$ decays) representative of the breaking of the isospin symmetry. Results have been obtained in the $A = 31$ [19] and $A = 67$ [20] mirrors. Measuring branching ratios, multipole mixing ratios and lifetimes for all transitions involved in the mirror decays, $B(E1)$ values have been determined, allowing the extraction of the induced isoscalar components for both systems. For mass $A = 31$, using the experimentally determined $B(E1)$ strength for the mirror $7/2^-_1 \rightarrow 5/2^+_2$ transitions, i.e. 1135.6 keV in ^{31}P and 1163.9 keV in ^{31}S—Fig. 5—it leads to an isovector component of $\langle J_i|||M_{IV}|||J_f\rangle = 0.149(38)$ efm and an "induced" isoscalar component of $\langle J_i|||M_{IS}|||J_f\rangle = 0.021(2)$ efm. For the $A = 67$ mirror nuclei, one can deduce $\langle J_i|||M_{IV}|||J_f\rangle = 2.9(6) \times 10^{-3}$ efm and $\langle J_i|||M_{IS}|||J_f\rangle = 0.9(6) \times 10^{-3}$ efm. For both systems the comparison of the $B(E1)$ strengths in the two mirror transitions indicates a violation of the isospin symmetry manifested by the presence of a large induced isoscalar component. Self-consistent calculations using the NNLOsat [21] and using the Equation of Motion Phonon Method (EMPM) reproduce well the experimental findings, confirming the breaking of the isospin symmetry originating from the violation of the charge symmetry of the two- and three-body parts of the potential [19]. The results provides evidence for a coherent contribution to isospin mixing, probably involving the isovector giant monopole resonance [19,20]. A microscopic description of the mixing of isospin within the EMPM approach using the isospin formalism for expressing the hole-phonon basis is ongoing. We underline here the importance of the full completion of the AGATA project for pushing the limits for isospin-mixing determination to low and high mass N=Z and mirror systems. The rapid decrease in production cross section for selfconjugate and mirror nuclei for increasing masses can be compensated by the increase in efficiency and angular coverage of the detector, both essential characteristics for reaching the sensitivity required by such precision measurements. The crucial element here is the position sensitiveness of the array, essential for enlarging the range of achievable lifetimes (sub-fantosecond times) as well as the capability of providing accurate angular distribution and linear polarisation information.

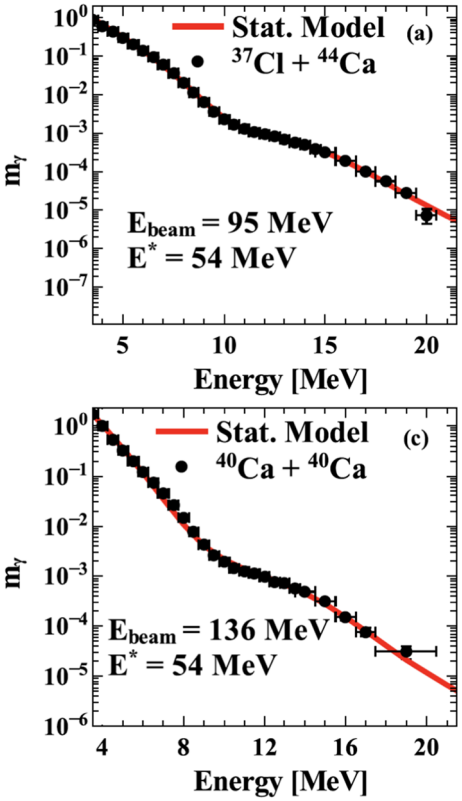

Fig. 3 High-energy γ-ray spectra for the reactions ^{37}Cl + ^{44}Ca (**a**) and ^{40}Ca + ^{40}Ca (**c**). The data, measured with LaBr3:Ce detectors and AGATA, are shown with full circles in comparison with the best-fitting statistical model calculations (red lines). Taken from Ref. [17]

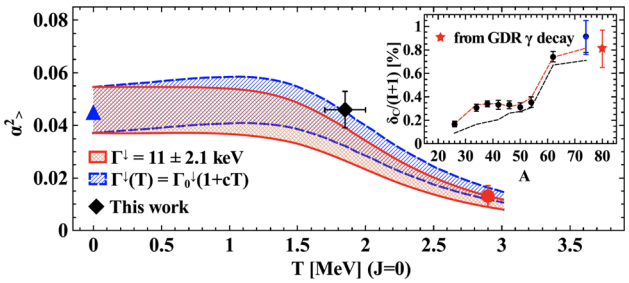

Fig. 4 The isospin mixing α^2 as a function of temperature. The blue triangle is the theoretical value at zero temperature, the red circle is the datum from Ref. [18], and the black diamond is the datum for ^{80}Zr. The inset gives the isospin mixing correction δc as a function of the nuclear mass A. Taken from Ref. [17]

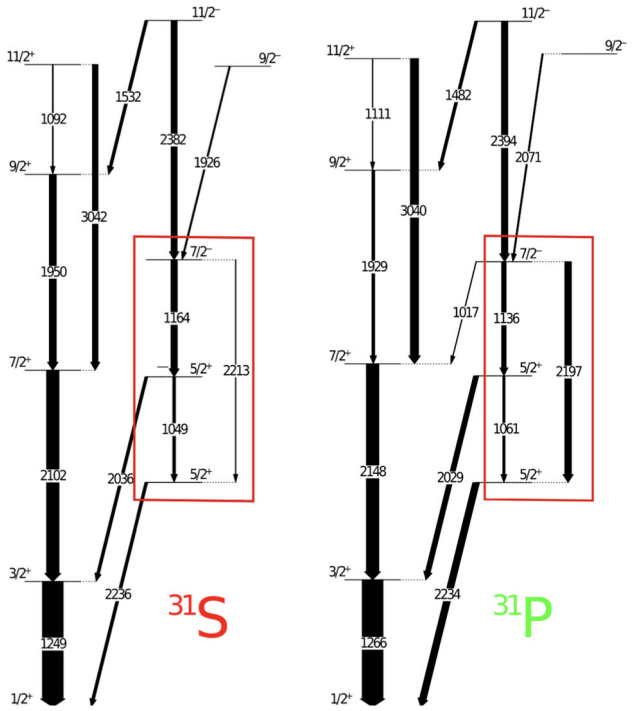

Fig. 5 Partial level scheme of ^{31}S and ^{31}P from Ref. [19] up to spin $11/2^-$. Only the yrast cascades of the two nuclei are shown. The width of the arrows is proportional to the relative intensities of the transitions. The different pattern of the decay of the $7/2^-$ states in the mirror couple is clearly seen (levels surrounded by rectangles)

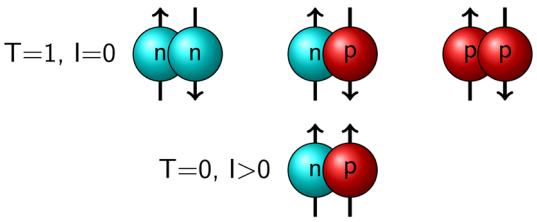

Fig. 6 Schematic illustration of the four possible types of pair correlations between neutrons and protons in an atomic nucleus. The arrows indicate the coupling of the nucleonic spins within a pair. The upper row shows the normal situation in stable or near-stable atomic nuclei. There, neutrons normally only pair with neutrons and protons only pair with protons. According to the Pauli principle of quantum mechanics, the particles in the equal pairs must have antialigned spins because the wave function is isospin-symmetric (isospin $T = 1$). There is also a possibility that a neutron-proton pair could have isospin 1, the middle pair in the top row. Below is shown the new type of pair correlations between neutrons and protons with isospin zero that seem to be able to occur in very unstable atomic nuclei with equal numbers of neutrons and protons. For these isoscalar pair correlations, the Pauli principle requires parallel spins within a neutron-proton pair, which can give rise to completely new phenomena in, for example, rotating atomic nuclei

2.2 Pair correlations and their isospin modes

Nucleonic pair correlations play an important role for the structure of atomic nuclei, reflected also in their gross properties such as radii and masses. Well-known manifestations of such correlations, which have similarities with superconductivity and superfluidity in condensed matter physics (BCS theory [22,23]), are the odd-even staggering of nuclear masses [24], seniority symmetry [25–27] in the low-lying spectra of spherical even-even nuclei, and the reduced moments of inertia and backbending effect [28,29] in rotating deformed nuclei.

Among the bound many-body systems found in Nature atomic nuclei uniquely are built from a coexistence of two distinct fermionic systems (neutrons and protons). A striking example of the importance of this coexistence is that out of the three possible combinations of neutron/proton two-body systems only the deuteron is bound. Nuclei may therefore exhibit additional pairing phenomena not found elsewhere in Nature.

In nuclei with equal numbers of neutrons and protons ($N = Z$) enhanced correlations arise between them since they, apart from their isospin projection, T_3, carry the same quantum numbers. Such correlations may favour an unusual type of nuclear superfluidity, *isoscalar* neutron-proton (np) pairing [30–33] in addition to the normal isovector ($T = 1$) pairing mode based on like-particle neutron-neutron (nn) and proton-proton (pp) Cooper pairs. Neutrons and protons may here also form np $T = 1$ (isovector), angular momentum $I = 0$ pairs, see Fig. 6.

Of special interest is the long-standing question of the possibility of an np pairing condensate [30–36] built primarily or partially from isoscalar $T = 0$, $I > 0$ np pair correlations. The occurrence of a significant component of $T = 0$ correlated np pairs in the nuclear wave function is also likely to have other interesting implications, e.g. the proposed "isoscalar spin-aligned np coupling scheme" in the heaviest, spherical, $N = Z$ nuclei [37].

The experimental fingerprints of np pairing are complex and there is most likely no single "smoking gun". There is still insufficient experimental evidence to unambiguously conclude on the presence of a significant component of isoscalar, $T = 0$, np pairing from the currently known properties of low- or high-spin states in even-even $N = Z$ nuclei. However, the available data for the heavier $N = Z$ nuclei is quite limited due to the severe experimental challenges: Accurate information on masses for $N = Z$ nuclei above $A \approx 80$ is currently out of reach, shape coexistence effects have muddled the analysis of rotational patterns of deformed $N = Z$ nuclei in the mass $A \sim 70$ region, and np transfer reaction studies on the lighter $N = Z$ nuclei are suffering from the complexity in the interpretation of the experimental results. Furthermore, correlations of this type are enhanced in heavier nuclei where more particles in high-j shells can participate and where the production cross sections in fusion, multi-nucleon transfer or fragmentation reactions are exceedingly small.

The best place to look for evidence of an isoscalar pairing condensate is predicted to be in nuclei with $A > 80$ [38–40]. Already in the 1990s it was realised from calculations using isospin-generalised Bardeen-Cooper-Schrieffer (BCS) equations and Hartree-Fock-Boguliubov (HFB) theory, including pp, nn, np ($T = 1$), and np ($T = 0$) Cooper pairs that there may exist a second-order quantum phase transition in the ground states of $N = Z$ nuclei from $T = 1$ pairing below mass 80 to a predominantly $T = 0$ pairing phase above mass 90, with the intermediate mass 80–90 region showing a co-existence of $T = 0$ and $T = 1$ pairing modes [41]. A ground-state pairing condensate dominated by $T = 0$ correlations has even been predicted in $N \sim Z$ nuclei around mass 130 [42] although such exotic nuclei are currently not experimentally accessible.

The interplay between rotation and the $T = 1$ pairing condensate has been studied during several decades in deformed nuclei in different mass regions. Since, normally, the neutron and proton Fermi levels are situated in different quantum shells neutrons and protons can be considered to form separate Fermi liquids dominated by strong $T = 1$ pair correlations. However, in self-conjugate or near-self-conjugate systems the isoscalar, $T = 0$, np pairing mode might appear as discussed above. As the spin-aligned coupling is allowed and even favoured in an isoscalar-paired system it has the interesting property of being less perturbed by the Coriolis interaction in a rotating system, which tends to break the time reversed pairs. The presence of an np pairing condensate may therefore be expressed in the properties of rotational structures in deformed $N = Z$ nuclei. This has been studied theoretically within the framework of isospin-generalised cranking model [43] and HFB calculations [44], the latter suggesting a mixed $T = 1/T = 0$ pairing phase with a transition from $T = 1$ to $T = 0$ dominance as a function of increasing angular momentum in the nucleus $^{80}_{40}Zr_{40}$. In a deformed, rotating nucleus the first $T = 1$ quasiparticle alignments typically occur at rotational frequencies in the range $\hbar\omega = 0.2 - 0.5$ MeV. If a significant component of $T = 0$ pairs is present in the wave functions of the corresponding states, measurable effects on the rotational patterns (backbends/upbends) should result. Intermediate-angular momentum states of rotating $N = Z$ nuclei therefore appear to be among the best places to search for the presence of $T = 0$ np pairing. Theory also indicates that it is important to study the heaviest possible $N = Z$ nuclei where, however, the experimental conditions are most challenging. One of the key signatures proposed for isoscalar pairing is a significant "delay" in band crossing frequency in deformed $N = Z$ isotopes compared with their $N > Z$ neighbours [45], which necessitates the study of such nuclei up to angular momentum around $I = 10\hbar$ or higher [38]. Such effects have previously been observed in the deformed $N = Z$ nuclei $^{72}_{36}Kr_{36}$, $^{76}_{38}Sr_{38}$, and $^{80}_{40}Zr_{40}$ but do not constitute conclusive evidence for isoscalar np-pairing effects due to the theoretically predicted possibility of shape changes occurring at similar rotational frequencies as the quasiparticle alignments [45–47].

The nuclei $^{84}_{42}Mo_{42}$ and $^{88}_{44}Ru_{44}$ also had indications of delays in the rotational alignments, however in these cases the previously available experimental data did not reach the required rotational frequency in order to draw firm conclusions [48,49]. While the situation concerning ^{84}Mo is still the same, the low-lying yrast structure of ^{88}Ru, predicted to be the heaviest deformed, self-conjugate nucleus that is bound, was recently studied and extended with AGATA [39] as discussed below.

Low-lying level structures of the extremely neutron-deficient $T_3 = 0\,(N = Z)$ $^{88}_{44}Ru_{44}$ and $T_3 = 1/2\,(N = Z+1)$ $^{87}_{43}Tc_{44}$ have recently been studied using the combination of AGATA, the NEDA and Neutron Wall neutron detector arrays [50], and the DIAMANT [51] charged particle detector array. The excited states were populated via the ^{54}Fe(^{36}Ar, 2n/p2n)^{88}Ru/^{87}Tc fusion-evaporation reactions at the Grand Accélérateur National d'Ions Lourds (GANIL) accelerator complex. The structure of its intermediate-to-high-spin states constitutes one of the most promising cases for discovering effects of a BCS-type of isoscalar pairing condensate. However, due to the large experimental difficulties in producing and selecting such exotic nuclei in sufficient quantities excited states in ^{88}Ru were previously known only up to the $I^\pi = 8^+$ state [48], just where normal (isovector) paired band crossings are expected to appear in the absence of strong isoscalar pairing. The observed γ-ray cascades in the AGATA-GANIL experiment were assigned to ^{88}Ru and ^{87}Tc using clean prompt γ-γ-2-neutron coincidences in coincidence/anti-coincidence with the detection of charged particles, confirming and extending the previously assigned sequences of low-lying excited states [39,40,52]. For ^{88}Ru, the observed low-lying yrast structure is consistent with a moderately deformed rotating system exhibiting a band crossing at a rotational frequency that is significantly higher than standard theoretical predictions based on isovector pairing, as well as observations in neighbouring even-even $N > Z$ nuclides [39], see Fig. 7. The direct observation of such a *delayed* rotational alignment in a deformed $N = Z$ nucleus is in agreement with theoretical predictions related to the presence of strong isoscalar neutron-proton pair correlations. On the other hand, for ^{87}Tc the constructed yrast level structure exhibits a rotational behaviour with a sharp backbending at $\hbar\omega \approx 0.50$ MeV [40] (Fig. 8). A *decrease* in alignment frequency and increase in alignment sharpness in the odd-mass isotonic chains around $N = 43$ is proposed as a new effect of the enhanced isoscalar neutron-proton interactions in odd-mass nuclei when approaching the $N = Z$ line [40]. Further characterisation of intermediate-angular momentum states of the heaviest self-conjugate nuclei and

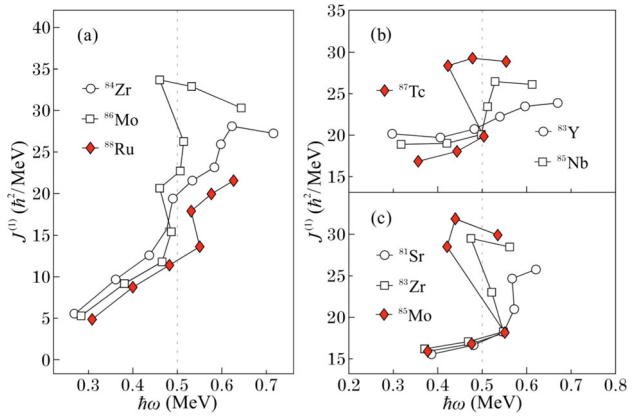

Fig. 7 Moments of inertia as a function of rotational frequency of the positive-parity yrast bands in $N = 44$ odd-even and even-even [39,53,54] isotones. The black dashed vertical line indicates the approximate rotational frequency of the first isovector-paired band crossing due to $g_{9/2}$ protons as predicted by standard cranked shell model calculations [55,56]. Taken from Ref. [40]

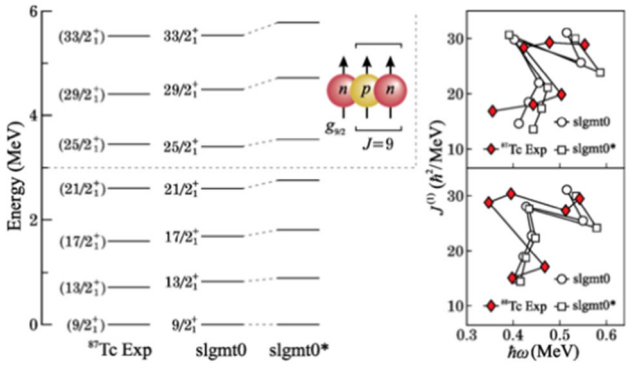

Fig. 8 Left: The experimental level scheme of ^{87}Tc in comparison with the shell-model calculations in the pg model space based on the slgmt0 [57] interaction (slgmt0* denotes the calculation with the spin-aligned neutron-proton interaction reduced by 200 keV). The cartoon illustrates the coupling between the unpaired neutron with the spin-aligned np pair which is the dominant component of the wave function for the higher-spin states. Right: Kinematic moments of inertia as a function of rotational frequency for the positive parity and positive signature bands in ^{87}Tc [40] and ^{89}Tc [58] from the experimental data and theoretical calculations (slgmt0 and slgmt0*). Taken from Ref. [40]

their closest neighbours as well as lifetime measurements of their low-lying excited states are crucial for understanding the neutron-proton pairing mode. This will require the significant step in sensitivity provided by AGATA in its 3–4π configuration.

3 Rotating nuclei at extreme deformation, mass, and charge

Deformation is an emergent mesoscopic property of the atomic nucleus, which consists of a finite quantum system of strongly interacting fermions. It arises as a spontaneous breaking of spherical symmetry similar to the Jahn-Teller effect in molecules [59]. It is driven by the occupation of quantum levels in anisotropic orbits with large values of orbital angular momentum ℓ, which occurs for particle numbers away from the spherical closed-shell magic numbers. Hence nuclei with incomplete quantum shells tend to adopt a deformed prolate spheroidal *quadrupole* shape, with one of the principal axes longer than the other two (equal) axes.

The deformed shape allows rotational excitation in nuclei as discussed by Bohr and Mottelson which led to their reception of the Nobel Prize in 1975. The evolution of nuclear structure with increasing angular momentum has recently been summarised in Ref. [60]. With rapid rotation, particular nuclear shapes with simple integer axes ratios of 3:2, 4:3, 2:1, 3:1 are predicted to provide extra stability and represent *deformed* shell gaps or new magic numbers at enhanced quadrupole deformation. These shapes correspond to a much larger deformation than a typical nuclear ground state and are further stabilised at high angular momentum, or rotational frequency.

Superdeformed (SD) shapes, corresponding to a 2:1 axes ratio, are now well established across the nuclear landscape [61], with more than 350 SD bands known to date. Superdeformation was originally discovered at high spin in 1984 in ^{152}Dy [62], via the observation of two-dimensional γ-ray energy correlations (called ridges) measured with the TESSA2 multidetector array of 6 Compton-suppressed Ge detectors. Subsequently, long cascades of regularly spaced discrete gamma-ray transitions were observed in ^{152}Dy [63], ^{132}Ce [64], and later in the mass 190 region [65]. These experiments used modest γ-ray spectrometers and the analysis was limited to two-dimensional correlations $E(\gamma 1)$ vs $E(\gamma 2)$. The energy spacing of the γ rays within these structures implied enhanced moments of inertia and hence large deformation. Subsequent measurements of the mean lifetimes [66–68], and hence electric quadrupole moments, of the decaying levels indeed showed that they corresponded to shapes with enhanced quadrupole deformation. Many other examples of SD shapes are now known in nuclei of different mass regions [61] thanks to the higher-efficiency γ-ray spectrometers such as Euroball and Gammasphere, which allowed analysis of triple and quadruple correlations.

These superdeformed bands represent the most striking example of shape-coexistence in the atomic nucleus. The description of the properties of highly elongated systems in terms of a SD well separated from the normal-deformed (ND) minimum by a potential barrier is confirmed by several experimental probes, the most important related to the existence of linking transitions directly connecting the bands built in the two separate wells. However, only in a very limited number of cases have such transitions been identified, therefore energy, spins and parities of the SD bands remain mostly undeter-

mined. In mass 150 [69] and 190 nuclei [70–76], for example, the decay out from SD bands occurs through very energetic (3–5 MeV) discrete transitions, carrying only a percent fraction of the intensity of the SD band, which otherwise decays via highly fragmented two-, three-and higher-order step cascades, resulting in quasi-continuum distributions governed by chaotic properties [77,78]. The discrete high-energy linking transitions are usually affected by large Doppler shifts and are poorly detected in standard HPGe detectors. The Doppler reconstruction capabilities of AGATA will help in highlighting such weak transitions, bringing the observation limit into the highly fragmented decay strength of the SD bands.

Another important subject which has experienced much progress, thanks to the combination of multi-detector Compton-suppressed arrays and efficient recoil separators, concerns the spectroscopy of deformed heavy transactinide nuclei. These species are extremely difficult to study in prompt γ-ray spectroscopy due to the low production cross-section and the high fission background. A recent review and related challenges can be found in Ref. [79]. The first evidence of a rotational band in a deformed transfermium element was found in ^{254}No [80,81] in experiments performed at Argonne National Laboratory with the Gammasphere array and at the University of Jyväskylä with the SARI multi-detector array. The observation of γ-ray transitions up to spin 14 and 16$\hbar$ respectively surprisingly showed that the shell effects, which are largely responsible for the fission stability, are robust against rotation. Again, with powerful γ-ray spectrometers coupled to state-of-the-art separators, it will be possible to explore and study in detail the structure of very heavy and super heavy elements (VHE/SHE) in the future.

Over the years, the nucleus ^{158}Er has been studied with most of the arrays mentioned above [60]. Figure 9 illustrates the time evolution of the spectrometers in terms of the experimental sensitivity to the detection of weak transitions and, correspondingly, to the highest spin reached in this nucleus. As discussed in Ref. [82], it demonstrates the power of bigger arrays and the unique capabilities of γ-ray tracking arrays such as AGATA and GRETA.

In the following, we will give some physics examples that can only be addressed with the AGATA γ-tracking device.

3.1 Triaxial nuclear shapes

Another class of large deformation structures has been established in rare-earth nuclei around mass 160 [83]. These have been interpreted in terms of *triaxial strongly deformed* (TSD) shapes where all three principal axes differ in length. This nuclear shape, with no axis of symmetry, is then able to perform a new mode of excitation–precession or *wobbling* motion. Nuclear wobbling motion was initially discussed by Bohr and Mottelson [84], where this type of rotation requires

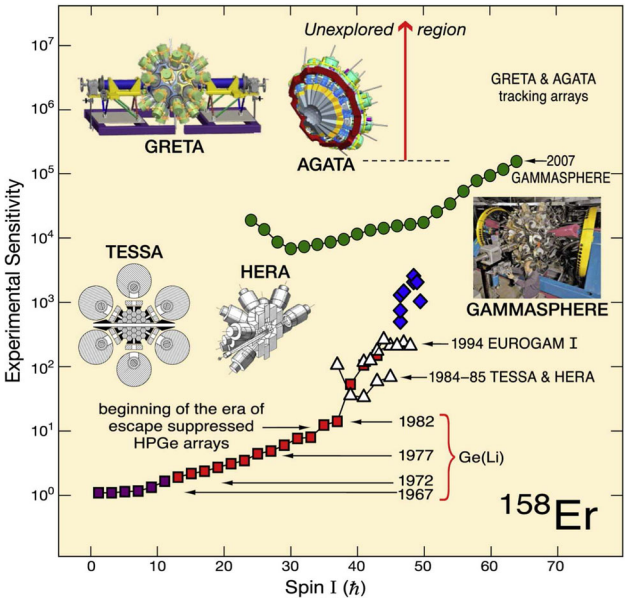

Fig. 9 The evolution of the power to detect states in ^{158}Er as new germanium detection arrays were built and became available [60]. The y-axis provides the sensitivity of the arrays, which is the inverse of the smallest γ ray intensity that can be observed, and the x-axis indicates the highest spins that was observed with the spectrometers indicated in the figure. Taken from Ref. [60]

a triaxially deformed nuclear shape (with *long*, *short*, and *intermediate* axes). In this wobbling mode the nucleus rotates around the principal axis having the largest moment of inertia and this axis executes harmonic oscillations (*precesses*) about the space-fixed angular momentum vector. Its analogue in classical mechanics is the motion of a free asymmetric top, while in quantal systems a corresponding example would be the rotation of molecules having different moments of inertia for the three principal axes.

TSD bands have been established at very high spin in ^{157,158}Er using high-fold γ^6 correlations [85,86] and, through comparison to theory [87], may extend discrete-line gamma-ray spectroscopy up to 75$\hbar$. It is also possible that some of these bands represent wobbling motion [88]. The high-spin deformed triaxial shape is similar to a classical Jacobi shape of a self-gravitating liquid.

The increased efficiency of the AGATA spectometer should allow future studies of very high-spin states in atomic nuclei, pushing into the *ultrahigh-spin* regime, to be possible through high-fold γ-ray analysis.

3.2 New hopes for hyperdeformation

Calculations based on the cranking-Strutinsky method, with a deformed Woods-Saxon potential [89], predicted in 1988 the existence of extremely elongated hyperdeformed nuclear shapes with axes ratios significantly exceeding 2:1. Several

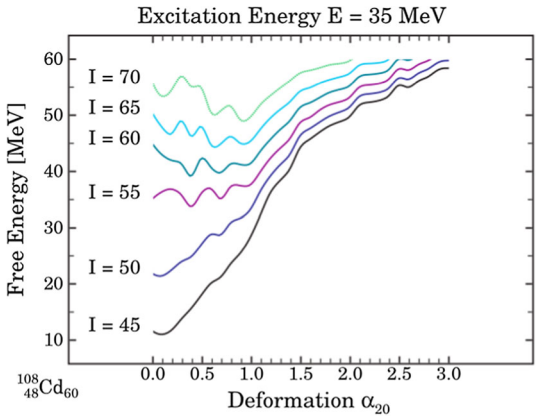

Fig. 10 Total free energy of ^{108}Cd as a function of the quadrupole elongation for an excitation energy of 35 MeV, characteristic of low temperatures. Taken from Ref. [92]

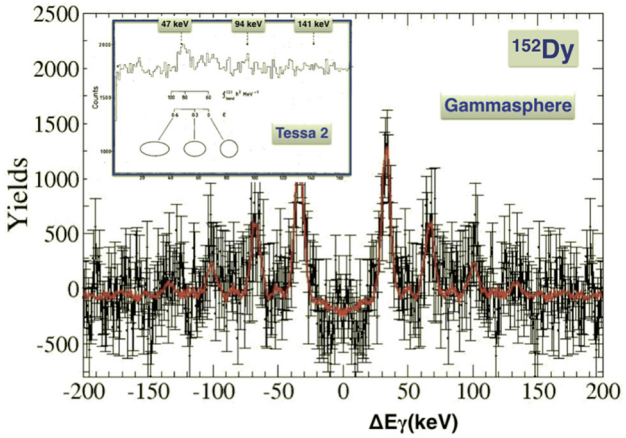

Fig. 11 Ridges obtained when coincidence gates are placed on clean pairs of SD γ rays in ^{152}Dy from an experiment performed with Gammasphere. One can see at least four narrow ridges as well as a shallow valley. The solid line is from Monte-Carlo calculations [96]. The inset shows the same ridge structure as measured for the first time with Tessa2 [62] before the identification of the the discrete SD band in ^{152}Dy

experiments [90,91] aimed at finding evidence for nuclear hyperdeformation (HD) were performed with Gammasphere and Euroball during two decades, and none of them were successful. In general the observation of very deformed nuclei requires favourable experimental conditions such as input angular momentum and excitation energy together with reliable theoretical predictions.

Whereas superdeformation is stabilised by strong shell effects, the HD shell-effects are not comparably strong [89]. Only those nuclei which show a near Jacobi transition, and for which the liquid-drop energy minimum is thus shifted towards large deformations, can be populated as HD states. As a consequence, this phenomenon can only occur at very high, and within a narrow window of angular momentum and possibly in very few nuclei. Guided by theoretical predictions, systematic searches for HD, and the Jacobi transition, have been made in Hf, Nd, Ba, Xe, Sn, and Cd nuclei over a decade. The analysis of the long Euroball experiment [90], showed that a discrete HD yrast band intensity will be significantly less than 1 part in 10^6 of the strongest bands populated in the reaction. The precise location of the islands of hyperdeformed nuclei and the experimental conditions needed to populate these exotic structures are still unknown. The chain of Cd isotopes is very interesting [92,93], with ^{108}Cd being one of the most promising candidate for the planning of future experiments.

Calculations, shown in Fig. 10, suggest that there exists a competition among SD and HD minima at an angular momentum $I \sim 60\hbar$, where the minima have nearly the same excitation energy. In this context, the authors of Ref. [92], suggest that perhaps selecting events which decay along the SD band could purify the condition for finding hyperdeformed structures at even higher spins. This is only possible with 4π high-efficiency, high-granularity detectors such as AGATA and GRETA for such a complex discrete spectroscopy where one selects the sequence of interest by gating on SD states which already represent at most 2% of the total cross-section in fusion-evaporation reactions.

Another promising hunting ground for HD using γ-tracking arrays could be the quasi-continuum ridge analysis (see Sect. 4 for more details). Indeed, in a region where the level density is high, $E2$ γ-ray transitions are no longer simply intraband transitions, because the level spacing is smaller than the matrix elements of the residual interaction (i.e., two or more body interactions beyond the mean field treatment) [94]. Moreover, with the high resolving power and tracking capabilities of AGATA, it will be possible to perform experiments in calorimetric (e.g adding up all energies) and discrete modes at the same time. This represents a new hope for the observation of HD structures selecting events on the basis of measured total γ-ray sum-energy H and multplicity k [94] (i.e. the distribution of the entry points in the excitation energy versus spin plane) while high-spin discrete data is sorted and thereby control the feeding of the quasi-continuum and discrete bands. It is also possible that hyperdeformation will only manifest itself in ridges in the continuum and no discrete hyperdeformed bands may ever be observed. Figure 11 clearly demonstrates the effect of the resolving power with a bigger array compared with Tessa2: AGATA will be at least 10 times better than Gammasphere. Note that measuring the (H, k) distribution with γ-ray tracking may represent a challenge but as shown in Ref. [94], when using simulated data and from recent measurement with GRETINA, the newly developed techniques for γ-ray tracking arrays are promising [95].

It is also expected that the use of exotic, neutron-rich, species to induce fusion-evaporation reactions will help in

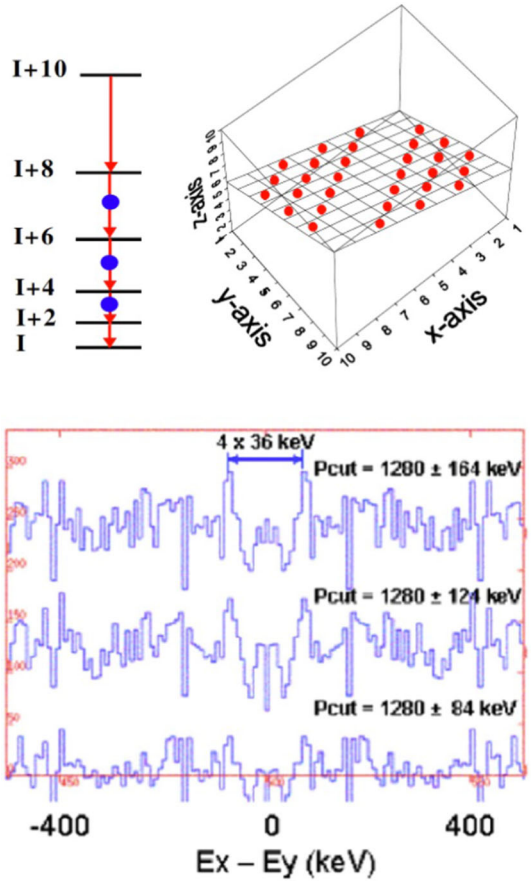

Fig. 12 Top Panel: Schematic representation of the so-called "rotational plane", obtained from three-dimensional histograms (with the energy correlation condition $E_{\gamma_1}+E_{\gamma_2}=2E_{\gamma_3}\pm\delta$), selecting rotational cascades of at least 3 consecutive transitions. Bottom panel: rotational plane projections (perpendicular to the main diagonal, at the average energy 1280 keV and width ±84, ±124, ±164 keV) in ^{128}Xe, populated by the ^{64}Ni+^{64}Ni→^{128}Ba fusion evaporation reaction, performed with Euroball at Strasbourg. Ridge structures associated with very large moment of inertia are consistent with hyperdeformed shapes. Figure adapted from Ref. [91], under CC Licence

populating higher spins, given the increase of the fission barrier with increasing number of neutrons. This will then allow to populate high-spin states at relative low-excitation energy, reaching the SD and HD pockets more effectively than with the use of stable beams [97]. First indications of possible HD structures were indeed obtained from the analysis of ridges associated to large moment of inertia, as observed in projections of multidimensional histograms obtained in the highest statistics experiment performed with the Euroball array coupled with the DIAMANT charged particle detector (see Fig. 12). The coupling of AGATA, in its Phase-II configuration, to post-accelerated exotic beams at energies of 5–10 MeV/A is therefore the best combination for such studies to be performed.

3.3 Detailed spectroscopy of superheavy nuclei

The existence of SHE nuclei is a striking manifestation of shell effects, which create a pocket in the potential energy surface of the nucleus, protecting it against spontaneous fission. The rotational properties of deformed super heavy systems constitute an excellent laboratory to test modern mean-field theory in extreme conditions of mass and charge, far away from the ones where the effective forces have been adjusted [98,99]. It is also important to determine the limiting spin and excitation energy that these nuclei can sustain as these data provide valuable information on the fission barriers which govern their survival probability in the nuclear reactions used to synthesise them. Meta stable states, or *isomers*, corresponding to high-K configurations, are prevalent throughout the nuclear chart. Here K is a quantum number that represents the projection of the total nuclear angular momentum onto the symmetry axis of a deformed nucleus. Due to the coexistence of low and high-j single-particle orbitals at the Fermi surface, K-isomers are a common feature in the transfermium region. Studying the electromagnetic and rotational properties of the bands built upon the isomers can shed light on their underlying quasiparticle structure, pairing correlations and the mechanisms by which angular momentum is generated. However, to date, only two such bands have been successfully studied [100,101]. These high-K states are also of special interest since a growing body of data seem to indicate that, despite their large excitation energies (>= 1 MeV), they experience a considerable hindrance to fission as compared with the ground state. The possibility that K-isomers could be more stable than the ground states in super heavy elements has been discussed recently [102].

Because it can be produced with the highest production cross section in the region (∼3μb), the most studied transfermium nucleus is ^{254}No. The first observation of its ground-state rotational band [80,81] firmly established that the nucleus is deformed (4:3 axes ratio) and constituted an important confirmation of predictions. This band was later extended up to spin 24$\hbar$ with the combination of JUROGAM and the RITU recoil separator at Jyväskylä [103]. The data also revealed other weaker rotational structures and discrete high-energy lines, which so far could not be placed in the level scheme of ^{254}No. Later on, using Gammasphere in its calorimetric mode coupled to the FMA [104], the systematic measurement of the (H, k) distributions of ^{254}No nuclei as a function of increasing beam energy [105,106] allowed to deduce a fission barrier height of B_f = 6.0(5) MeV at spin 15$\hbar$. More recently, thanks to the clover detectors of the SAGE array [107], a linear polarisation analysis of enhanced high-energy γ rays emitted by ^{254}No provided the first experimental evidence of a scissors mode in such a heavy system [108]. The combination of the resolving power, calorimetric efficiency with superior energy resolution and polarisation

sensitivity of AGATA and state-of-the art recoil separators, will allow to pursue such varied spectroscopic studies at the sub-μ barn level. Moreover, the unprecedented high resolution of AGATA will also enable an excellent Doppler correction and hence the observation of the highest possible spins. Figure 13 of Ref. [109] shows a nice example of the expected statistics and data quality for ^{254}No with AGATA. In order to gain some understanding about the single-particle shell structure and the dynamics of super heavy nuclei, the investigation of the properties of odd-N and/or odd-Z heavy elements is essential. However, such studies are particularly challenging due to the small cross sections and the spread of the population intensity over multiple bands. This is the reason why only 3 odd-Z isotopes and one odd-N isotope beyond fermium have been investigated to high spin [110–115]. These problems can only be overcome by combining AGATA to an appropriate residual nucleus identification and by taking advantage of the current high-rate capabilities of AGATA and the foreseen improvements in overall throughput.

4 Warm rotation at high spin

The atomic nucleus is one of the best examples of a finite many-body quantum system for which the interplay between collective and single-particle degrees of freedom can be used to probe the gradual evolution toward a chaotic regime [116–118]. At low internal energies, the level scheme of a nucleus shows specific patterns determined by the active shells and orbitals, the overall deformation, and the interaction between closely lying orbitals. As the internal energy increases further, together with a reduced level spacing, it becomes more difficult to resolve specific configurations which start to interact strongly. In the compound nucleus regime, well established quantum numbers lose their meaning, and the nucleus acts as a chaotic quantum system [119]. The intermediate regime, where the order-to-chaos transition occurs, is not fully established, with some evidence of persistence of quantum numbers up to 1.5–2 MeV of internal excitation energy, in medium/heavy mass nuclei [120–122]. The standard analysis technique is based on the investigation of quasi-continuum spectra originating from rotating nuclei at high spins and moderate excitation energies [116–118].

Figure 13 (bottom) schematically illustrates the decay pattern of warm rotating nuclei, in the excitation energy-angular momentum phase space [126]. The zoom, on the top, illustrates the generation of complex stationary states, which are at the basis of the onset of the order-to-chaos transition in atomic nuclei, together with the fragmentation of the rotational $E2$ strength over an energy range, named Γ_{rot} [123], that leads to quasi-continuum energy distributions [125].

The different rotational regimes that are expected, depending on the order-chaos properties of the intrinsic states and of

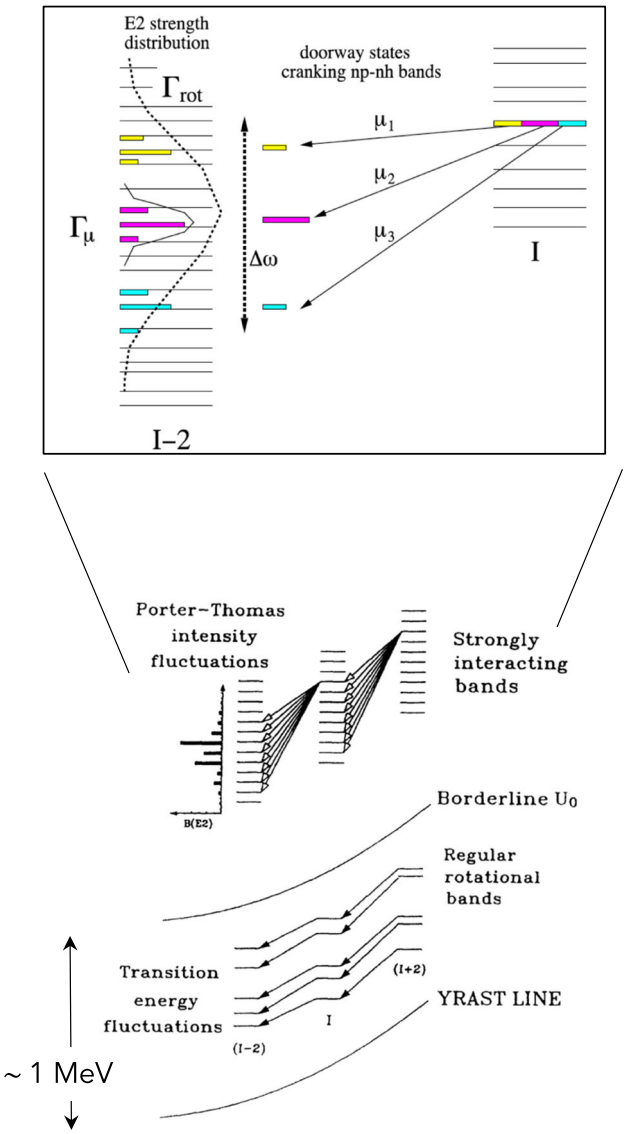

Fig. 13 Bottom: Schematic representation of the γ-decay pattern in the excitation energy-angular momentum phase space. The region of discrete, regular rotational bands (ordered motion) and the regime of strongly interacting bands (at the onset of chaos) are indicated. Top: Detailed illustration of the fragmentation of the rotational $E2$ strength from a state at spin I to a number of final states at spin $(I-2)$, owing to the complex nature of the nuclear states already at few hundreds keV excitation energy above the yrast line. The FWHM of the distribution at $(I-2)$ is called rotational damping width, Γ_{rot} [123]. The μ_i values are $np-np$ unperturbed "shell model" bands, mixed by the residual interaction over the Γ_μ energy range (i.e., the compound nucleus spreading width) to form a state at spin I. The dispersion $\Delta\omega$ in rotational frequency, from spin I to spin $(I-2)$ originates from the different response to rotation of each unperturbed band. Adapted from [124,125]

the rotational motion, are presented in Fig. 14, as highlighted in Ref. [127]. In addition to the regular motion along "discrete bands" (typical of the order regime), and to the "rotational damping regime" of highly fragmented decay of strongly mixed bands (a precursor of the fully chaotic regime), the very peculiar situation of so-called "ergodic bands" is also

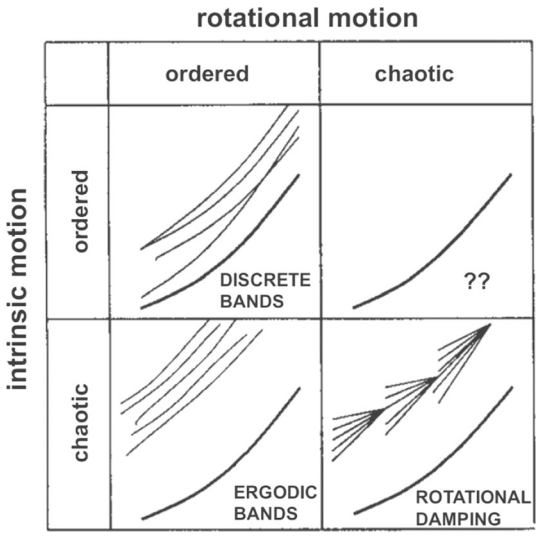

Fig. 14 The different rotational regimes that are observed in rotating nuclei, depending on the order-chaos properties of intrinsic states and of the rotational motion. The case of intrinsic ordered motion and chaotic rotational motion is expected to be not realistic for nuclear systems. See text for details. Adapted from [127]

shown in the figure [128]. The latter can arise when fully mixed states display coherent rotational motion. In this case, the band mixing does not lead to a damping of the rotational motion, since the admixture of the wave function changes very slowly with angular momentum.

4.1 Experimental access to quasi-continuum

The study of warm rotating nuclei has been based, so far, on a series of experiments performed with large arrays equipped with Compton-Suppression Shields, such as Euroball, Gammasphere and their precursors [116–118]. Quasi-continuum rotational spectra have been investigated in multi-dimensions, exploiting double and triple coincidences between γ rays emitted in the decay [118,129,130], statistical fluctuations methods [131], as well as simulations of the entire γ-decay flow, also based on microscopic cranked shell model calculations at finite temperature [132–134]. Figure 15 illustrates how the typical ridge-valley pattern, in two-dimensional histograms, emerges from $\gamma-\gamma$ rotational correlations, providing basic information of average properties of warm rotating nuclei: while the ridges are populated by discrete, yet non resolved, transitions, the valley is composed of transitions from closely lying, strongly interacting bands, from the rotational damping regime [127]. We note here that first indications of the existence of highly deformed structures (superdeformed and possibly also hyperdeformed) were obtained from the analysis of ridges associated to large moment of inertia [62,90] (see Sect. 3).

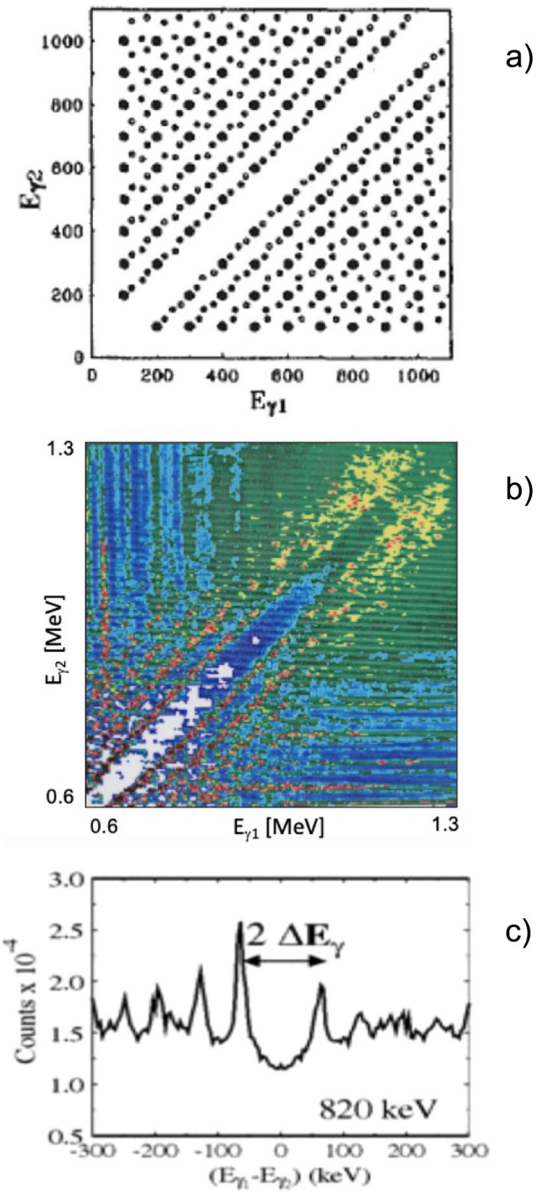

Fig. 15 **a** Illustration of the emergence of rotational correlations in $\gamma-\gamma$ coincidence matrices from rotating nuclei at high spins. Regular rotational bands (e.g., the yrast and discrete excited bands, see Fig. 13) generate ridge structures running parallel to the $E_{\gamma_1} = E_{\gamma_2}$ diagonal (panel **a**)), while the fragmented rotational decay from strongly mixed bands, gives rise to a rather uniform distribution filling also the valley region. **b** $\gamma-\gamma$ spectrum of ^{168}Yb (0.6−1.3 MeV region, 1 keV/ch), obtained with the Eurogam I array [135]. **c** projection of the ^{168}Yb $\gamma-\gamma$ matrix, perpendicular to the $E_{\gamma_1} = E_{\gamma_2}$ diagonal, at the average transition energy 820 ± 30 keV. The distance between the two most inner ridges depends on the moment of inertia $\mathcal{J}^{(2)}$, being $\Delta E_\gamma = \hbar^2/2\mathcal{J}^{(2)}$. For $E_{\gamma_1} > E_{\gamma_2}$ the intensity associated to known discrete rotational bands has been subtracted from the $\gamma-\gamma$ matrix, leading to the asymmetric ridge structure. The remaining ridge intensity corresponds to discrete bands, not yet resolved. Adapted from [116,118]

With arrays based on Compton-Suppression Shields, average properties of the order-to-chaos transition in the atomic

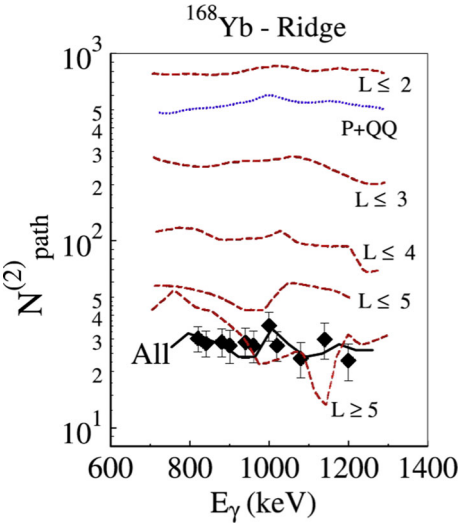

Fig. 16 The experimental number of two-steps discrete bands in ^{168}Yb, named "paths" (diamond symbols), as extracted from the analysis of count fluctuations of the ridge structures of $\gamma - \gamma$ coincidence spectra, in comparison with expected values from band mixing calculations at finite temperature (lines). Different L-multiple decomposition of the two-body residual interaction, of SDI type, are shown, as well as results using a pairing plus quadrupole force (P+QQ) (dotted line). (Figure adapted from [118])

nucleus have been investigated for a number of rare-earth nuclei around mass $A = 160$, and in superdeformed systems with mass $A = 150$ and 180. In all cases, only a partial observation of discrete rotational bands forming ridge structures has been possible. Precursors to ergodic rotational bands have been reported in just one case, the superdeformed nucleus ^{194}Hg [136]. In addition, few rare examples of discrete transitions associated to the fragmentation of the rotational decay, at the onset of the rotational damping regime, have been clearly identified [137].

The intrinsic characteristic of the AGATA array, given its unprecedented peak-to-total and increased efficiency for high-multiplicity events, will help making a significant step forward in the research of the physics of the quasi-continuum. AGATA is expected to provide complete γ-ray spectroscopy with the identification of all levels and transitions belonging to rotational bands populating the ridge structures, up into the rotational damping regime (see Figs. 13 and 15).

In the following, we provide selected examples of quasi-continuum investigations which will strongly profit from the enhanced sensitivity of tracking arrays.

4.2 Onset of chaos: impact of two-body residual interaction and mass dependence

With tracking arrays, such as AGATA, establishing quantum numbers and selection rules for all states and γ decay modes of discrete (and ergodic) rotational bands will become feasible, as well as identifying a large fraction of the fragmented decay strength, in terms of discrete transitions. This will lead to a detailed experimental description of the onset of the order to chaos in rotating nuclei. In turn, by comparison with microscopic calculations, specific properties of the two-body residual interaction will be highlighted [138]. As shown in Fig. 16, the number of discrete "paths" (i.e., two-steps discrete bands) populating the ridge structures in a typical rare-earth nucleus (e.g., ^{168}Yb), as measured in early experiments with Compton Suppressed HPGe arrays, is found to be strongly sensitive to the characteristics of the two-body term of the residual interaction. It follows that this investigation, performed on a larger sample of nuclear systems and in different regions of the nuclear chart, could become instrumental in benchmarking most recent effective nucleon-nucleon interactions, as a function of internal excitation energy, possibly including also three-body terms of the nuclear force. The latter have been recently shown to play a significant role in describing a number of nuclear structure features in light to heavy systems [139–142]. By performing such studies in different mass regions, a major step forward in the understanding of the nuclear force will be achieved. So far, the gradual onset of chaos and the dependence of the rotational damping width with mass, for example, has been addressed only comparing results from nuclei in $A = 110$ to $A = 160$ [143] (see Fig. 17), while the contributions of single neutron and proton components are still to be defined. As shown in Fig. 18, in Yb isotopes the rotational damping width Γ_{rot} (black circles) is expected to increase ~25% from A = 168 to A = 176, mostly due to neutron shell effects [138]. This will be clarified with the use of reactions induced by exotic beams, helping to populate long isotopic chains. In this respects, a key reaction will be ^{132}Sn on ^{48}Ca, allowing to populate ^{176}Yb up to $76\hbar$, with an average excitation almost 1 MeV higher than achievable with stable beams.

4.3 Conservation of the K quantum number with temperature

The K quantum number, defined as the projection onto the symmetry axis of the total angular momentum, in a deformed nucleus, can be used to establish the extent of the validity of quantum numbers intrinsic of a rotational nucleus, as a function of the internal excitation energy. The existence of long-living isomeric states is the typical signature of validity of selection rules limiting the decay between bands characterised, for example, by large differences in the K number [144]. The isomer existence arises from the approximate conservation of K. In an electromagnetic de-excitation, if K were a good quantum number, the change in K should not exceed λ, the transition multipole order. Transitions that violate this rule are called K forbidden. In reality, rather than strictly

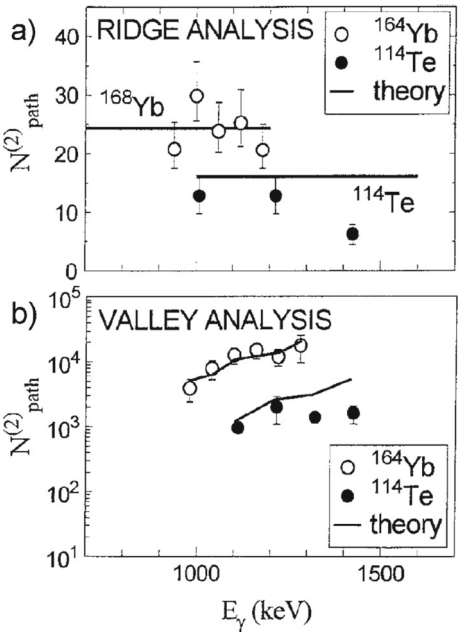

Fig. 17 The number of two-steps decay paths, $N^{(2)}_{path}$, extracted from the fluctuation analysis of the measured first ridge (panel (**a**)) and valley (panel (**b**)) of ^{164}Yb (open circles) and ^{114}Te (full circles) nuclei, in comparison with predictions from band mixing calculations (full lines). (Figure Adapted from [143])

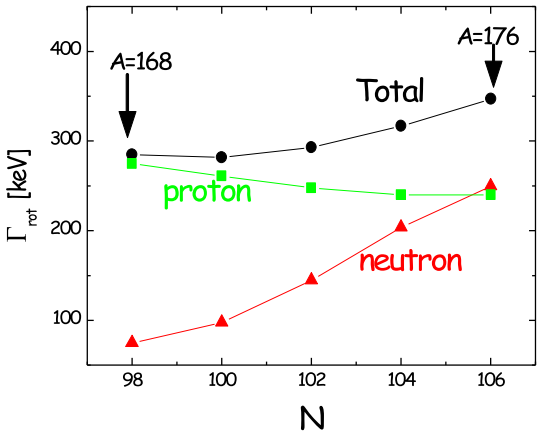

Fig. 18 The contribution to the total rotational damping width, Γ_{rot}, in Yb isotopes (A = 168 to 176) is given separately for protons and neutrons. The calculations are performed at spin I = 40$\hbar$ and thermal energy U∼2 MeV. (Figure adapted from [138])

forbidden, such transitions are strongly hindered, resulting in long-lived isomeric states.[1]

From the studies of several highly K-forbidden $E1$ transitions from multi-quasiparticle isomers in the $A = 170$ mass region, it emerges, as key feature, that the inhibition declines for isomers that are at higher excitation energy, relative to a rigid rotor of the same total angular momentum. This is because of different K-mixing mechanisms, such as rotational (Coriolis) mixing, loss of axial symmetry, and level density effects with increasing internal excitation energy [145].

To achieve a more comprehensive picture of the K-mixing phenomenon, it is important to gather complementary information from the decay properties of the entire body of discrete (and fragmented) excited high-K bands, forming quasi-continuum ridge-valley structures in $\gamma-\gamma$ correlation matrices. This approach was employed in a few experiments, performed with arrays using Compton Suppression Shields, aiming at the study of the average properties of γ-decay fluxes feeding low-K and high-K rotational bands in ^{163}Er [121]. A persistence of strong K-selection rules was reported for excited rotational bands forming the ridges, characterised by energies up to ≈ 0.8 MeV above yrast line, while in the rotational damping region, a smaller mixing was found, due to the residual interaction, for high-K bands, thus pointing to a progressive weakening of selection rules on K, with increasing internal energy U.

AGATA, with its large efficiency and resolving power, is expected to allow a significant advancement in these studies. A first exploratory experiment of this type was conducted with the AGATA Demonstrator at LNL [2], where four AGATA triple clusters were coupled to a multiplicity filter array (HELENA) composed of 27 BaF_2 detectors. The presence of the multiplicity filter allowed the selection of high-fold events, related to long cascades starting at high spins. The experiment used a fusion-evaporation reaction leading to $^{173-174}$W, as main residues [122]. The analysis of quasi-continuum spectra of ^{174}W, employing techniques similar to the ones developed for the pioneering case of ^{163}Er, confirmed, also in this case, the persistence of selection rules for K around 1 MeV of internal energy. In addition, for the first time, reduced hindrance factors f_ν, as a function of internal energy U, were estimated for the $E1$ decay between high-K and low-K discrete excited bands up into the band mixing region. As shown in Fig. 19, the results obtained for f_ν are consistent with the reduced hindrance values extracted from the analysis of discrete high-K isomers in the $A = 160-180$ mass region [147], thus confirming the important role of level density in the determination of K-forbidden transition rates.

The exploratory work on ^{174}W, performed with the AGATA Demonstrator, was hampered by the limited efficiency of the array, of about 5%, and— more strongly— by the limited granularity of the system, not allowing to achieve high statistics for high-coincidence data. New studies with improved tracking-array performances are therefore needed, also exploiting intense radioactive beams which will increase the pool of nuclei to be addressed and will help also disentangling specific contributions of the residual interaction, depending on protons and neutrons, for example.

[1] The reduced hindrance factor is defined as $f_\nu = F_W^{1/\nu}$, where F_W is the ratio of the Weisskopf estimate to the measured transition rates and $\nu = \Delta K - \lambda$ is the degree of forbiddenness.

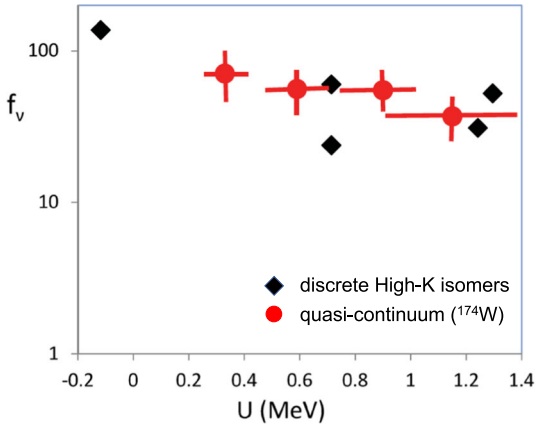

Fig. 19 Reduced hindrance f_ν, for $E2$ decay from selected discrete high-K isomers in ^{164}Er ($K^\pi = 12^+$), ^{174}Yb ($K^\pi = 14^+$), ^{174}Hf ($K^\pi = 14^+$; two decay branches) and ^{182}Hf ($K^\pi = 13^+$) (black diamonds) ([146] and Refs. therein), in comparison with the quasicontinuum analysis performed in ^{174}W with the AGATA Demonstrator [122]. Adapted from Ref. [145]

5 Summary and conclusions

Fusion-evaporation reactions have been crucial in populating excited states in nuclei over the years. Current aspects of nuclear structure have been reviewed and new possibilities discussed with the AGATA γ-ray tracking spectrometer.

Acknowledgements We thank the AGATA collaboration for its scientific support to this manuscript. This work has been supported in part by the United Kingdom Science and Technology Facilities Council under grants ST/P004598/1 and ST/V001027/1. The authors are grateful to the following laboratories where the research described in this manuscript was performed: Laboratori Nazionali di Legnaro, Hubert Curien Multi-disciplinary Institute Strasbourg, Argonne National Laboratory, GANIL, Jyvaskyla laboratory, Daresbury laboratory and Lawrence Berkeley National Laboratory.

Funding Information Open access funding provided by Università degli Studi di Milano within the CRUI-CARE Agreement.

Data Availability Statement This manuscript has no associated data or the data will not be deposited. [Authors' comment: The data presented in this manuscript has been already published before, therefore there are no data associated with it.]

References

1. S. Akkoyun et al., Nucl. Instrum. Methods Phys. Res. A **668**, 26 (2012). https://doi.org/10.1016/j.nima.2011.11.081
2. A. Gadea et al., Nucl. Instrum. Methods Phys. Res. A **654**, 88 (2011). https://doi.org/10.1016/j.nima.2011.06.004
3. N. Pietralla et al., EPJ Web Conf. **66**, 02083 (2014). https://doi.org/10.1051/epjconf/20146602083
4. E. Clément et al., Nucl. Instrum. Methods Phys. Res. A **855**, 1 (2017). https://doi.org/10.1016/j.nima.2017.02.063
5. J.J. Valiente-Dobón et al., Nucl. Instrum. Methods Phys. Res. A **1049**, 168040 (2023). https://doi.org/10.1016/j.nima.2023.168040
6. S. Paschalis et al., Nucl. Instrum. Methods Phys. Res. A **709**, 44 (2013). https://doi.org/10.1016/j.nima.2013.01.009
7. R. Machleidt, I. Slaus, J. Phys. G **27**, R69 (2001). https://doi.org/10.1088/0954-3899/27/5/201
8. M.A. Bentley, S.M. Lenzi, Prog. Part. Nucl. Phys. **59**, 497 (2007). https://doi.org/10.1016/j.ppnp.2006.10.001
9. E.K. Warburton, J. Weneser, in *Isospin in Nuclear Physics*. ed. by D.H. Wilkinson (North-Holland Publishing Company, 1969), pp.173–228
10. A.J.F. Siegert, Phys. Rev. **52**, 787 (1937). https://doi.org/10.1103/PhysRev.52.787
11. G. Gosta et al., Phys. Rev. C **103**, L041302 (2021). https://doi.org/10.1103/PhysRevC.103.L041302
12. W. Satuła, J. Dobaczewski, M. Konieczka, W. Nazarewicz, (2013). arXiv:1307.1550v1.pdf
13. W. Satuła, J. Dobaczewski, W. Nazarewicz, M. Rafalski, Phys. Rev. Lett. **103**, 012502 (2009). https://doi.org/10.1103/PhysRevLett.103.012502
14. E. Farnea et al., Phys. Lett. B **551**, 56 (2003). https://doi.org/10.1016/S0370-2693(02)03022-8
15. N.S. Kelsall et al., Phys. Rev. C **64**, 024309 (2001). https://doi.org/10.1103/PhysRevC.64.024309
16. H. Iwasaki et al., Phys. Rev. Lett. **112**, 142502 (2014). https://doi.org/10.1103/PhysRevLett.112.142502
17. S. Ceruti et al., Phys. Rev. Lett. **115**, 222502 (2015). https://doi.org/10.1103/PhysRevLett.115.222502
18. A. Corsi et al., Phys. Rev. C **84**, 041304 (2011). https://doi.org/10.1103/PhysRevC.84.041304
19. D. Tonev et al., Phys. Lett. B **821**, 136603 (2021). https://doi.org/10.1016/j.physletb.2021.136603
20. R. Orlandi et al., Phys. Rev. Lett. **103**, 052501 (2009). https://doi.org/10.1103/PhysRevLett.103.052501
21. A. Ekström et al., Phys. Rev. C **91**, 051301 (2015). https://doi.org/10.1103/PhysRevC.91.051301
22. J. Bardeen, L.N. Cooper, J.R. Schrieffer, Phys. Rev. **106**, 162 (1957). https://doi.org/10.1103/PhysRev.106.162
23. J. Bardeen, L.N. Cooper, J.R. Schrieffer, Phys. Rev. **108**, 1175 (1957). https://doi.org/10.1103/PhysRev.108.1175
24. W. Heisenberg, Z. Phys. **78**, 156 (1932)
25. A. de Shalit, I. Talmi, *Nuclear Shell Theory* (Academic Press, New York, 1963)
26. I. Talmi, *Simple Models of Complex Nuclei* (Harwood Academic Press, Switzerland, 1993)
27. D.J. Rowe, G. Rosensteel, Phys. Rev. Lett. **87**, 172501 (2001). https://doi.org/10.1103/PhysRevLett.87.172501
28. A. Johnson, H. Ryde, J. Sztarkier, Phys. Lett. B **34**, 605 (1971). https://doi.org/10.1016/0370-2693(71)90150-X
29. F.S. Stephens, R.S. Simon, Nucl. Phys. A **183**, 257 (1972). https://doi.org/10.1016/0375-9474(72)90658-6
30. J. Engel, K. Langanke, P. Vogel, Phys. Lett. B **389**, 211 (1996). https://doi.org/10.1016/S0370-2693(96)01294-4

31. J. Engel, S. Pittel, M. Stoitsov, P. Vogel, J. Dukelsky, Phys. Rev. C **55**, 1781 (1997). https://doi.org/10.1103/PhysRevC.55.1781
32. O. Civitarese, M. Reboiro, P. Vogel, Phys. Rev. C **56**, 1840 (1997). https://doi.org/10.1103/PhysRevC.56.1840
33. A.L. Goodman, Adv. Nucl. Phys. **11**, 263 (1979)
34. W. Satuła, R. Wyss, Phys. Rev. Lett. **87**, 052504 (2001). https://doi.org/10.1103/PhysRevLett.87.052504
35. G. Martínez-Pinedo, K. Langanke, P. Vogel, Nucl. Phys. A **651**, 379 (1999). https://doi.org/10.1016/S0375-9474(99)00141-4
36. D.D. Warner, M.A. Bentley, P. Van Isacker, Nat. Phys. **2**, 311 (2006). https://doi.org/10.1038/nphys291
37. B. Cederwall et al., Nature **469**, 68 (2011). https://doi.org/10.1038/nature09644
38. S. Frauendorf, A.O. Macchiavelli, Prog. Part. Nucl. Phys. **78**, 24 (2014). https://doi.org/10.1016/j.ppnp.2014.07.001
39. B. Cederwall et al., Phys. Rev. Lett. **124**, 062501 (2020). https://doi.org/10.1103/PhysRevLett.124.062501
40. X. Liu et al., Phys. Rev. C **104**, L021302 (2021). https://doi.org/10.1103/PhysRevC.104.L021302
41. A.L. Goodman, Phys. Rev. C **60**, 014311 (1999). https://doi.org/10.1103/PhysRevC.60.014311
42. A. Gezerlis, G.F. Bertsch, Y.L. Luo, Phys. Rev. Lett. **106**, 252502 (2011). https://doi.org/10.1103/PhysRevLett.106.252502
43. W. Satuła, R. Wyss, Phys. Lett. B **393**, 1 (1997). https://doi.org/10.1016/S0370-2693(96)01603-6
44. A.L. Goodman, Phys. Rev. C **63**, 044325 (2001). https://doi.org/10.1103/PhysRevC.63.044325
45. G. de Angelis et al., Phys. Lett. B **415**, 217 (1997). https://doi.org/10.1016/S0370-2693(97)01217-3
46. S.M. Fischer et al., Phys. Rev. Lett. **87**, 132501 (2001). https://doi.org/10.1103/PhysRevLett.87.132501
47. P.J. Davies et al., Phys. Rev. C **75**, 011302 (2007). https://doi.org/10.1103/PhysRevC.75.011302
48. N. Mărginean et al., Phys. Rev. C **63**, 031303 (2001). https://doi.org/10.1103/PhysRevC.63.031303
49. N. Mărginean et al., Phys. Rev. C **65**, 051303 (2002). https://doi.org/10.1103/PhysRevC.65.051303
50. J.J. Valiente-Dobón et al., Nucl. Instrum. Methods Phys. Res. A **927**, 81 (2019). https://doi.org/10.1016/j.nima.2019.02.021
51. J.N. Scheurer et al., Nucl. Instrum. Methods Phys. Res. A **385**, 501 (1997). https://doi.org/10.1016/S0168-9002(96)01038-8
52. X. Liu et al., Phys. Rev. C **106**, 034304 (2022). https://doi.org/10.1103/PhysRevC.106.034304
53. H.G. Price, C.J. Lister, B.J. Varley, W. Gelletly, J.W. Olness, Phys. Rev. Lett. **51**, 1842 (1983). https://doi.org/10.1103/PhysRevLett.51.1842
54. D. Rudolph et al., Phys. Rev. C **54**, 117 (1996). https://doi.org/10.1103/PhysRevC.54.117
55. K. Jonsson et al., Nucl. Phys. A **645**, 47 (1999). https://doi.org/10.1016/S0375-9474(98)00603-4
56. J. Dudek, W. Nazarewicz, N. Rowley, Phys. Rev. C **35**, 1489 (1987). https://doi.org/10.1103/PhysRevC.35.1489
57. F.J.D. Serduke, R.D. Lawson, D.H. Gloeckner, Nucl. Phys. A **256**, 45 (1976). https://doi.org/10.1016/0375-9474(76)90094-4
58. D. Rudolph et al., Nucl. Phys. A **587**, 181 (1995). https://doi.org/10.1016/0375-9474(94)00825-8
59. H.A. Jahn, E. Teller, Proc. R. Soc. Lond. A **161**, 220 (1937). https://doi.org/10.1098/rspa.1937.0142
60. M.A. Riley, J. Simpson, E.S. Paul, Phys. Scr. **91**, 123002 (2016). https://doi.org/10.1088/0031-8949/91/12/123002
61. B. Singh, R. Zywina, R.B. Firestone, Nucl. Data Sheets **97**, 241 (2002). https://doi.org/10.1006/ndsh.2002.0018
62. B.M. Nyakó et al., Phys. Rev. Lett. **52**, 507 (1984). https://doi.org/10.1103/PhysRevLett.52.507
63. P.J. Twin et al., Phys. Rev. Lett. **57**, 811 (1986). https://doi.org/10.1103/PhysRevLett.57.811
64. P.J. Nolan, A. Kirwan, D.J.G. Love, A.H. Nelson, D.J. Unwin, P.J. Twin, J. Phys. G **11**, L17 (1985)
65. E.F. Moore et al., Phys. Rev. Lett. **63**, 360 (1989). https://doi.org/10.1103/PhysRevLett.63.360
66. A.J. Kirwan, G.C. Ball, P.J. Bishop, M.J. Godfrey, P.J. Nolan, D.J. Thornley, D.J.G. Love, A.H. Nelson, Phys. Rev. Lett. **58**, 467 (1987). https://doi.org/10.1103/PhysRevLett.58.467
67. M.A. Bentley et al., Phys. Rev. Lett. **59**, 2141 (1987). https://doi.org/10.1103/PhysRevLett.59.2141
68. E.F. Moore et al., Phys. Rev. Lett. **64**, 3127 (1990). https://doi.org/10.1103/PhysRevLett.64.3127
69. T. Lauritsen et al., Phys. Rev. Lett. **88**, 042501 (2002). https://doi.org/10.1103/PhysRevLett.88.042501
70. T.L. Khoo et al., Phys. Rev. Lett. **76**, 1583 (1996). https://doi.org/10.1103/PhysRevLett.76.1583
71. A. Lopez-Martens et al., Phys. Lett. B **380**, 18 (1996). https://doi.org/10.1016/0370-2693(96)00367-X
72. G. Hackman et al., Phys. Rev. Lett. **79**, 4100 (1997). https://doi.org/10.1103/PhysRevLett.79.4100
73. K. Hauschild et al., Phys. Rev. C **55**, 2819 (1997). https://doi.org/10.1103/PhysRevC.55.2819
74. A.N. Wilson et al., Phys. Rev. Lett. **90**, 142501 (2003). https://doi.org/10.1103/PhysRevLett.90.142501
75. S. Siem et al., Phys. Rev. C **70**, 014303 (2004). https://doi.org/10.1103/PhysRevC.70.014303
76. A.N. Wilson et al., Phys. Rev. Lett. **95**, 182501 (2005). https://doi.org/10.1103/PhysRevLett.95.182501
77. A. Lopez-Martens et al., Phys. Rev. Lett. **77**, 1707 (1996). https://doi.org/10.1103/PhysRevLett.77.1707
78. A. Lopez-Martens et al., Nuclear Phys. A **647**, 217 (1999). https://doi.org/10.1016/S0375-9474(99)00012-3
79. D. Ackermann, Ch. Theisen, Phys. Scr. **92**, 083002 (2017). https://doi.org/10.1088/1402-4896/aa7921
80. P. Reiter et al., Phys. Rev. Lett. **82**, 509 (1999). https://doi.org/10.1103/PhysRevLett.82.509
81. M. Leino et al., Eur. Phys. J. A **6**, 63 (1999). https://doi.org/10.1007/s100500050318
82. A. Korichi, T. Lauritsen, Eur. Phys. J. A **55**, 121 (2019). https://doi.org/10.1140/epja/i2019-12787-1
83. S.W. Ødegård et al., Phys. Rev. Lett. **86**, 5866 (2001). https://doi.org/10.1103/PhysRevLett.86.5866
84. A.N. Bohr, B.R. Mottelson, *Nuclear Struct.* (World Scientific Publishing Company, UK, 1998). https://doi.org/10.1142/3530
85. E.S. Paul et al., Phys. Rev. Lett. **98**, 012501 (2007). https://doi.org/10.1103/PhysRevLett.98.012501
86. X. Wang et al., Phys. Lett. B **702**, 127 (2011). https://doi.org/10.1016/j.physletb.2011.07.007
87. A.V. Afanasjev, Y. Shi, W. Nazarewicz, Phys. Rev. C **86**, 031304 (2012). https://doi.org/10.1103/PhysRevC.86.031304
88. J. Simpson et al., Phys. Rev. C **107**, 054305 (2023). https://doi.org/10.1103/PhysRevC.107.054305
89. J. Dudek, T. Werner, L.L. Riedinger, Phys. Lett. B **211**, 252 (1988). https://doi.org/10.1016/0370-2693(88)90898-2
90. B. Herskind et al., AIP Conf. Proc. **701**, 303 (2004). https://doi.org/10.1063/1.1691723
91. B. Herskind et al., Acta Phys. Pol. B **38**, 1421 (2007). https://www.actaphys.uj.edu.pl/R/38/4/1421
92. N. Schunck, J. Dudek, B. Herskind, Phys. Rev. C **75**, 054304 (2007). https://doi.org/10.1103/PhysRevC.75.054304
93. H. Abusara, A.V. Afanasjev, Phys. Rev. C **79**, 024317 (2009). https://doi.org/10.1103/PhysRevC.79.024317
94. T. Lauritsen, A. Korichi, T.-L. Khoo, M.P. Carpenter, R.V.F. Janssens, L.A. Riley, D. Seweryniak, S. Zhu, Phys. Scr. **92**, 074002 (2017). https://doi.org/10.1088/1402-4896/aa709c
95. T. Lauritsen, A. Korichi, et al. To be published

96. T. Lauritsen et al., Phys. Rev. C **75**, 064309 (2007). https://doi.org/10.1103/PhysRevC.75.064309
97. P. Fallon, Acta Phys. Pol. B **36**, 1003 (2005). https://www.actaphys.uj.edu.pl/R/36/4/1003
98. M. Bender, P. Bonche, T. Duguet, P.-H. Heenen, Nucl. Phys. A **723**, 354 (2003). https://doi.org/10.1016/S0375-9474(03)01081-9
99. J. Dobaczewski, A.V. Afanasjev, M. Bender, L.M. Robledo, Y. Shi, Nucl. Phys. A **944**, 388 (2015). https://doi.org/10.1016/j.nuclphysa.2015.07.015
100. P.T. Greenlees et al., Phys. Rev. C **78**, 021303 (2008). https://doi.org/10.1103/PhysRevC.78.021303
101. B. Sulignano et al., Phys. Rev. C **86**, 044318 (2012). https://doi.org/10.1103/PhysRevC.86.044318
102. P.M. Walker, F.R. Xu, H.L. Liu, Y. Sun, J. Phys. G **39**, 105106 (2012). https://doi.org/10.1088/0954-3899/39/10/105106
103. R.-D. Herzberg, P.T. Greenlees, Prog. Part. Nucl. Phys. **61**, 674 (2008). https://doi.org/10.1016/j.ppnp.2008.05.003
104. C.N. Davids, J.D. Larson, Nucl. Instrum. Methods Phys. Res. B **40–41**, 1224 (1989). https://doi.org/10.1016/0168-583X(89)90624-1
105. P. Reiter et al., Phys. Rev. Lett. **84**, 3542 (2000). https://doi.org/10.1103/PhysRevLett.84.3542
106. G. Henning et al., Phys. Rev. Lett. **113**, 262505 (2014). https://doi.org/10.1103/PhysRevLett.113.262505
107. J. Pakarinen et al., Eur. Phys. J. A **50**, 53 (2014). https://doi.org/10.1140/epja/i2014-14053-6
108. F.L. Bello Garrote et al., Phys. Lett. B **834**, 137479 (2022). https://doi.org/10.1016/j.physletb.2022.137479
109. W. Korten et al., Eur. Phys. J. A **56**, 137 (2020). https://doi.org/10.1140/epja/s10050-020-00132-w
110. P. Reiter et al., Phys. Rev. Lett. **95**, 032501 (2005). https://doi.org/10.1103/PhysRevLett.95.032501
111. A. Chatillon et al., Phys. Rev. Lett. **98**, 132503 (2007). https://doi.org/10.1103/PhysRevLett.98.132503
112. R.-D. Herzberg et al., Eur. Phys. J. A **42**, 333 (2009). https://doi.org/10.1140/epja/i2009-10855-9
113. S. Ketelhut et al., Phys. Rev. Lett. **102**, 212501 (2009). https://doi.org/10.1103/PhysRevLett.102.212501
114. A.K. Mistry et al., Eur. Phys. J. A **53**, 24 (2017). https://doi.org/10.1140/epja/i2017-12215-8
115. R. Briselet et al., Phys. Rev. C **102**, 014307 (2020). https://doi.org/10.1103/PhysRevC.102.014307
116. S. Leoni, A. Lopez-Martens, Phys. Scr. **91**, 063009 (2016). https://doi.org/10.1088/0031-8949/91/6/063009
117. A. Lopez-Martens, T. Lauritsen, S. Leoni, T. Døssing, T.-L. Khoo, S. Siem, Prog. Part. Nucl. Phys. **89**, 137 (2016). https://doi.org/10.1016/j.ppnp.2016.02.003
118. A. Bracco, S. Leoni, Rep. Prog. Phys. **65**, 299 (2002). https://doi.org/10.1088/0034-4885/65/2/204
119. O. Bohigas, M.J. Giannoni, C. Schmit, Phys. Rev. Lett. **52**, 1 (1984). https://doi.org/10.1103/PhysRevLett.52.1
120. P. Bosetti et al., Phys. Rev. Lett. **76**, 1204 (1996). https://doi.org/10.1103/PhysRevLett.76.1204
121. G. Benzoni et al., Phys. Lett. B **615**, 160 (2005). https://doi.org/10.1016/j.physletb.2004.12.083
122. V. Vandone et al., Phys. Rev. C **88**, 034312 (2013). https://doi.org/10.1103/PhysRevC.88.034312
123. B. Lauritzen, T. Døssing, R.A. Broglia, Nucl. Phys. A **457**, 61 (1986). https://doi.org/10.1016/0375-9474(86)90519-1
124. S. Leoni et al., Phys. Rev. Lett. **93**, 022501 (2004). https://doi.org/10.1103/PhysRevLett.93.022501
125. S. Leoni et al., Phys. Rev. C **72**, 034307 (2005). https://doi.org/10.1103/PhysRevC.72.034307
126. B. Herskind et al., Phys. Rev. Lett. **68**, 3008 (1992). https://doi.org/10.1103/PhysRevLett.68.3008
127. T. Døssing, B. Herskind, M. Matsuo, S. Leoni, A. Bracco, E. Vigezzi, R.A. Broglia, Nucl. Phys. A **682**, 439 (2001). https://doi.org/10.1016/S0375-9474(00)00671-0
128. B.R. Mottelson, Nucl. Phys. A **557**, 717 (1993). https://doi.org/10.1016/0375-9474(93)90582-I
129. S. Leoni et al., Nucl. Phys. A **587**, 513 (1995). https://doi.org/10.1016/0375-9474(95)00024-U
130. S. Leoni, A. Bracco, T. Døssing, B. Herskind, J.C. Lisle, M. Matsuo, E. Vigezzi, J. Wrzesinski, Eur. Phys. J. A **4**, 229 (1999). https://doi.org/10.1007/s100500050224
131. T. Døssing, B. Herskind, S. Leoni, A. Bracco, R.A. Broglia, M. Matsuo, E. Vigezzi, Phys. Rep. **268**, 1 (1996). https://doi.org/10.1016/0370-1573(95)00060-7
132. A. Bracco, P. Bosetti, S. Frattini, E. Vigezzi, S. Leoni, T. Døssing, B. Herskind, M. Matsuo, Phys. Rev. Lett. **76**, 4484 (1996). https://doi.org/10.1103/PhysRevLett.76.4484
133. S. Leoni et al., Phys. Rev. C **79**, 064306 (2009). https://doi.org/10.1103/PhysRevC.79.064306
134. S. Leoni et al., Phys. Rev. C **79**, 064307 (2009). https://doi.org/10.1103/PhysRevC.79.064307
135. P.J. Nolan, Nucl. Phys. A **520**, c657 (1990). https://doi.org/10.1016/0375-9474(90)91182-Q
136. A. Lopez-Martens et al., Phys. Rev. Lett. **100**, 102501 (2008). https://doi.org/10.1103/PhysRevLett.100.102501
137. G.B. Hagemann et al., Nucl. Phys. A **618**, 199 (1997). https://doi.org/10.1016/S0375-9474(97)00056-0
138. M. Matsuo, T. Døssing, B. Herskind, S. Leoni, E. Vigezzi, R.A. Broglia, Phys. Lett. B **465**, 1 (1999). https://doi.org/10.1016/S0370-2693(99)01058-8
139. T. Otsuka, T. Suzuki, J.D. Holt, A. Schwenk, Y. Akaishi, Phys. Rev. Lett. **105**, 032501 (2010). https://doi.org/10.1103/PhysRevLett.105.032501
140. K. Hebeler, J.D. Holt, J. Menéndez, A. Schwenk, Annu. Rev. Nucl. Part. Sci. **65**, 457 (2015). https://doi.org/10.1146/annurev-nucl-102313-025446
141. M. Ciemała et al., Phys. Rev. C **101**, 021303 (2020). https://doi.org/10.1103/PhysRevC.101.021303
142. A. Gottardo et al., Phys. Rev. Lett. **109**, 162502 (2012). https://doi.org/10.1103/PhysRevLett.109.162502
143. S. Frattini et al., Phys. Rev. Lett. **83**, 5234 (1999). https://doi.org/10.1103/PhysRevLett.83.5234
144. P. Walker, G. Dracoulis, Nature **399**, 35 (1999). https://doi.org/10.1038/19911
145. P.M. Walker et al., Phys. Lett. B **408**, 42 (1997). https://doi.org/10.1016/S0370-2693(97)00819-8
146. Z. Patel et al., Phys. Lett. B **753**, 182 (2016). https://doi.org/10.1016/j.physletb.2015.12.026
147. P.M. Walker, Phys. Scr. **92**, 054001 (2017). https://doi.org/10.1088/1402-4896/aa694d